Thin-Walled Structures 109 (2016) 25–39

Contents lists available at ScienceDirect

Thin-Walled Structures

journal homepage: www.elsevier.com/locate/tws

Full length article

Behaviour of steel-jacket retrofitted RC columns with preload effects

An He [a], Jian Cai [a,b], Qing-Jun Chen [a,b,*], Xinpei Liu [c], Jin Xu [a]

[a] School of Civil Engineering and Transportation, South China University of Technology, Guangzhou 510640, PR China
[b] State Key Laboratory of Subtropical Building Science, South China University of Technology, Guangzhou 510640, PR China
[c] Centre for Infrastructure Engineering and Safety, The University of New South Wales, UNSW, Sydney 2052, Australia

ARTICLE INFO

Article history:
Received 29 December 2015
Received in revised form
9 September 2016
Accepted 9 September 2016

Keywords:
Steel jacket
Retrofit
RC column
Compression
Preloading
Fibre element

ABSTRACT

Steel jacketing is an efficient way to retrofit reinforced concrete columns. Previous studies focused on the performance improvement without considering the preloads on the original columns. The preloads might inevitably affect the structural performance of the retrofitted columns. Comprehensive experimental and numerical studies on the behaviour of steel-jacket retrofitted RC columns with preload effects are presented in this paper. Twenty-nine steel jacketing columns with different steel tube thicknesses, axial preloading levels and load eccentricities are tested under concentrically or eccentrically compressive loading.

The experimental results are discussed and illustrate that the effects of preloading levels on the axial compression strength of the retrofitted columns are negligible while increasing the preloads could decrease the eccentric compressive strength. A fibre element model is developed to predict the behaviour of the retrofitted columns. The material non-linear behaviour of all the components considering the steel tube and stirrup confining effects on the concrete as well as the preloading action are taken into account in the model. The model is validated by comparing its results with the experimental results. Extensive parametric studies are undertaken by using the proposed numerical model to elucidate the effects of axial and moment preloading and the effects of preloads with various other parameters on the performance of the retrofitted columns.

1. Introduction

For reinforced concrete (RC) structures, columns are amongst the most important components as far as vertical load transferring is concerned. Column members in older RC building or bridge may need to be retrofitted or repaired due to their long-term deteriorations as a result of exposure to adverse environmental conditions, or sometimes they need to be strengthened to satisfy the reconstruction demands. Several RC columns retrofitting solutions have been suggested, including fibre-reinforced polymer (FRP) composite wrapping, steel and concrete jacketing [1]. In deference to the others, the steel jacketing method is probably preferred because of its high retrofitting effectiveness and economic efficiency, as well as ease of construction. In this method, the common RC column is encased by a thin steel jacket (e.g. Fig. 1). The gap between the tube and the original column is filled with grout for integration purpose. The steel jacketing approach can provide more effective confinement on the concrete and significantly improve the strength, stiffness, and deformation capacity of the strengthened columns. The steel jacketing construction process is also quite efficient as the steel stub acting as permanent formwork. Surprisingly, there is limited research reported in the open literature on the investigation of RC column retrofitted by steel jacketing method. Chai *et al.* [2,3] studied the influence of steel jacketing on the lateral response of circular bridge columns. The results showed that the steel jacketing increased the lateral stiffness and ductility capacity of the columns. Priestley *et al.* [4,5] performed a comprehensive two-part study to determine the enhanced shear strength of columns provided by steel jacket retrofitting. Xiao *et al.* [6,7] conducted a series of tests on the columns with a square or rectangular section retrofitted by partially stiffened steel jackets and indicated the effectiveness of the proposed method. Li *et al.* [8] proposed a constitutive model to describe the behaviour of concrete confined by steel reinforcement, steel jackets and both steel reinforcement and steel jackets used to retrofit and strengthen RC structures. Choi *et al.* [9,10] introduced a new steel jacketing method with lateral pressure externally applied on steel jackets to tightly attach the jackets on concrete surfaces of columns, and thus did not require the grout used in conventional jacketing. It was found that the jackets could increase the ultimate strength, bond strength and ductility of the column specimens.

* Corresponding author at: School of Civil Engineering and Transportation, South China University of Technology, Guangzhou 510640, PR China.
E-mail address: qjchen@scut.edu.cn (Q.-J. Chen).

http://dx.doi.org/10.1016/j.tws.2016.09.013
0263-8231/

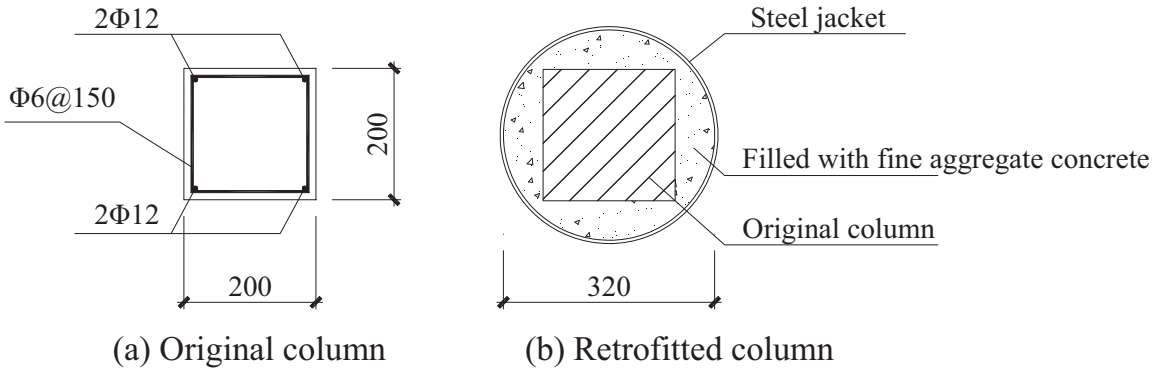

Fig. 1. Cross-sections of specimens. (a) Original column (b) Retrofitted column.

Table 1
Parameters and test results of specimens.

Specimen	t (mm)	e (mm)	η	P_u (kN)	Strength ratio
AZ1	–	0	–	990	1.00
BZ1	1.0	0	–	2202	2.22
BZ2	2.0	0	–	2990	3.02
BZ3	3.0	0	–	3820	3.86
BZ4	3.5	0	–	4180	4.22
BZ5	4.0	0	–	4460	4.51
BZ6	1.0	50	–	1728	1.75
BZ7	2.0	30	–	2540	2.57
BZ8	2.0	50	–	2108	2.13
BZ9	2.0	80	–	1797	1.82
BZ10	3.5	30	–	3450	3.48
BZ11	3.5	50	–	2636	2.66
BZ12	3.5	80	–	1850	1.87
CZ1	2.0	0	0.08	2780	2.81
CZ2	3.5	0	0.08	3678	3.72
CZ3	2.0	0	0.09	3030	3.06
CZ4	2.0	30	0.08	2040	2.06
CZ5	3.5	30	0.08	2741	2.77
CZ6	3.5	30	0.09	2988	3.02
CZ7	2.0	50	0.08	1727	1.74
CZ8	3.5	50	0.08	2190	2.21
CZ9	2.0	50	0.09	1980	2.00
CZ10	3.5	50	0.09	2136	2.16
DZ1	4.0	0	0.40	4290	4.33
DZ2	4.0	0	0.50	4230	4.27
DZ3	4.0	30	0.40	3380	3.41
DZ4	4.0	50	0.40	3000	3.03
DZ5	4.0	80	0.40	2560	2.59
DZ6	4.0	50	0.50	2920	2.95

Note: t is the thickness of steel jacket; e is the eccentricity from neutral axis; η is the preloading level and is defined as $\eta = P_{pre}/(f_{c1}A_n)$, where P_{pre} is the axial prestressed force on the original column, A_n is the net cross-sectional area of the original concrete; P_u is the experimental maximum load; strength ratio is the ratio of the value of P_u of each retrofitted column versus the value of P_u of unstrengthen column AZ1.

In practice, during the retrofitting construction, most of the pre-existing RC columns are subjected to preloads arising from the existing live and permanent loads from the upper floors or substructure. The stress and deformation induced by the preloads might inevitably affect the structural performance of the retrofitted columns. The effects of preloading on the behaviour of concrete-jacket retrofitted RC column have been addressed in some studies. Ersoy *et al.* [11] performed axial loading tests on concrete-jacket strengthened RC columns in both the preloaded and non-preload cases, and showed the ultimate strengths of the preloaded specimens were slightly lower than the non-preloaded ones. Takeuti *et al.* [12] presented rigorous experimental programme to evaluate the preload effects on the concrete jacketed columns, and stated that the preloading might not adversely affect the strength of the jacketed column but could reduce its deformability. Vandoros and Dritsos [13,14] compared the performance of preloaded and non-preloaded concrete jacketed RC columns under combined axial loading and bending moment. The comparison on the basis of flexural behaviour demonstrated the positive effects of preloading when considering the strength and deformation capacity although the preloading could reduce the initial stiffness. Recently, Papanikolaou *et al.* [15] analytically investigated the effects of core preloading on the strength of jacketed RC columns.

The purpose of this paper is to present experimental and numerical studies on the behaviour of steel-jacket retrofitted RC columns with preload effects. Tests of twenty-nine columns retrofitted by steel jackets subjected to concentrically or eccentrically compressive loading are reported and the experimental results are discussed. The variables among the tested specimens include the load eccentricity ratios, the thickness of steel tube and the axial preloading levels. A fibre element model using OpenSees software is proposed to predict the behaviour of the retrofitted columns. Both geometric and material non-linear behaviour of all the components and the preloading action are taken into account in the model. The model is validated by comparing its results with the experimental results. Parametric studies are then undertaken by using the proposed numerical model to further elucidate the effects of preloading on the performance of the retrofitted columns.

2. Experimental programme

2.1. Test specimens

Twenty-nine column specimens were fabricated and tested. The diameters of steel jackets D and the effective lengths of all the specimens were the same as 320 mm and 1000 mm respectively. The variables among the tested specimens include the thickness of steel tube t, the axial preloading levels η (the ratio of the axial preload to the predicted axial compressive strength of original column) and the load eccentricities e. Fig. 1 and Table 1 show the cross-sectional dimensions and the details of the specimens. The material properties are summarised in Table 2. In all the specimens, the unstrengthened one AZ1 was chosen as the control specimen. No preloads were applied on the specimens in Series BZ. The specimens in Series CZ were under relative low level of axial preloading from 0.08 to 0.09 while the one in series DZ were under relative high level of axial preloading from 0.4 to 0.5. The post-tensioned prestressing construction technique was implemented to simulate the preload actions on the specimens, as shown in Fig. 2. The original column was firstly fabricated with a pipe whose diameter is 36 mm along the central axis of the section. After 28 days concrete curing period, the steel bars were inserted into the pipe and the post-tensioning procedures were

Table 2
Material properties of components.

Specimen type	Concrete		Steel tube			Steel rebar		
	f_{c1} (MPa)	f_{c2} (MPa)	t (mm)	Yield strength (MPa)	Ultimate strength (MPa)	Diameter (mm)	Yield strength (MPa)	Ultimate strength (MPa)
AZ	27.6	–	–	–	–	6.0	305	440
BZ	27.6	25.7	1.0	312	376			
			2.0	306	440			
			3.0	278	392			
			3.5	304	422	12.0	386	575
			4.0	291	405			
CZ	20.2	22.0	2.0	273	355			
			3.5	307	456			
DZ	25.0	25.2	4.0	286	399			

Note: f_{c1}, f_{c2} are the axial compressive cylinder strengths of the original column concrete and infill concrete respectively, which are defined as 0.76 times of their characteristic cubic strengths.

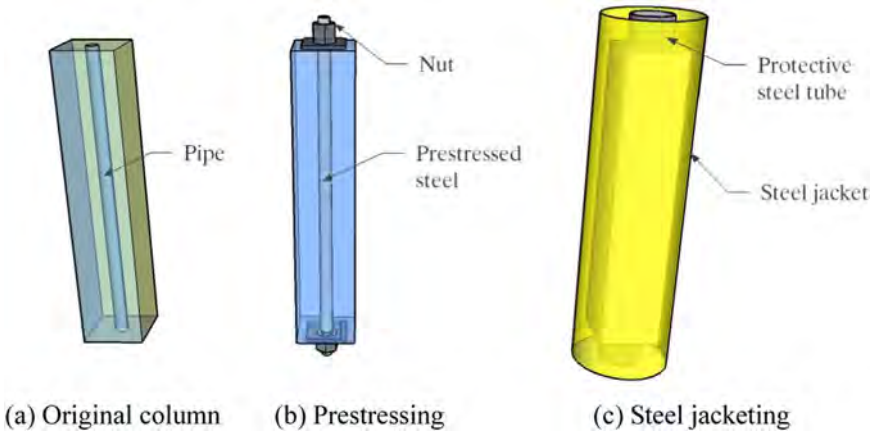

Fig. 2. Execution of specimens with preloading. (a) Original column (b) Prestressing (c) Steel jacketing.

carried out to apply compression on each side of the column. The prestressed column was then set in the middle of the steel jacket with two protective steel tubes locating at each end. The gap between the original column and the steel jacket was filled with fine aggregate concrete.

2.2. Test setup

The experimental test set-up and instrumentation are shown in Fig. 3. A 15,000 kN capacity compression testing machine was used for all the tests. The pin-connected boundary conditions were applied at both ends of specimens, for which the hemispherical bearings supports were adopted in the axial compression tests while the roller bearings supports were adopted in the eccentric compression tests. Load control at a constant speed of 4 kN/s was used prior to the yielding of steel tube. When the vertical strains of the steel tube reached the measured yield strain, displacement control loading at a constant rate of 0.005 mm/s was initiated. The tests were terminated when overlarge deformation and excessive local buckling were observed on the specimens.

Four linear variable differential transducers (LVDT#1 to LVDT#4) were arranged at each side of the specimens to measure the longitudinal deformations indicated as Δ_1–Δ_4 respectively. The longitudinal strains at each side of the specimens (defined as ε_1–ε_4) were calculated by dividing the deformations by the initial heights of the specimens. For the axial loaded specimens, the average longitudinal strain was obtained as the mean value of ε_1–ε_4. For the eccentrically loaded specimens, the curvature (φ) was determined by $|\varepsilon_1-\varepsilon_3|/b$, where b is the distance between LVDT#1 and LVDT#3. The mid-height lateral deflection of the specimens under eccentric compression was measured by LVDT#5.

3. Experimental results and discussions

3.1. Failure modes

For all the axial loaded specimens, their failure modes were similar as showed in Fig. 4(a) and (b). The shear slip lines firstly appeared when the axial compressive load reached about 60% of the maximum load, which indicated that the steel tubes began to yield. Obvious steel tube dilations were recognised at the peak load, following by the wrinkles appearing at the mid-height of the steel tubes and the shear slip lines were distributed all over the steel tube. The seriousness of the wrinkles increased with the increase of the steel tube thickness.

Typical compression-flexure failure mode was observed for all the eccentrically loaded specimens except for specimen BZ6 which failed due to welding fracture. When the applied loads reached about 60% of the maximum loads, the shear slip lines began to appear on the compression side of the steel tube (Fig. 4(c)). Local buckling of the steel tube (Fig. 4(d)) occurred in the vicinity of mid-height of specimen almost at the maximum applied load. Large mid-height lateral deflection could also be identified. No apparent difference between the failure modes of the non-preloaded and preloaded specimens was observed for both the loading cases.

3.2. Peak loads and load-deformation curves

The maximum experimental loads and the strength ratios of all the columns are listed in Table 1. It is shown that the peak loads increased proportionately as the thicknesses of steel tube increased for the columns with the same preload under the same experimental loading scenario. Fig. 5 presents the typical experimental load-strain responses of the control specimen AZ1 and the

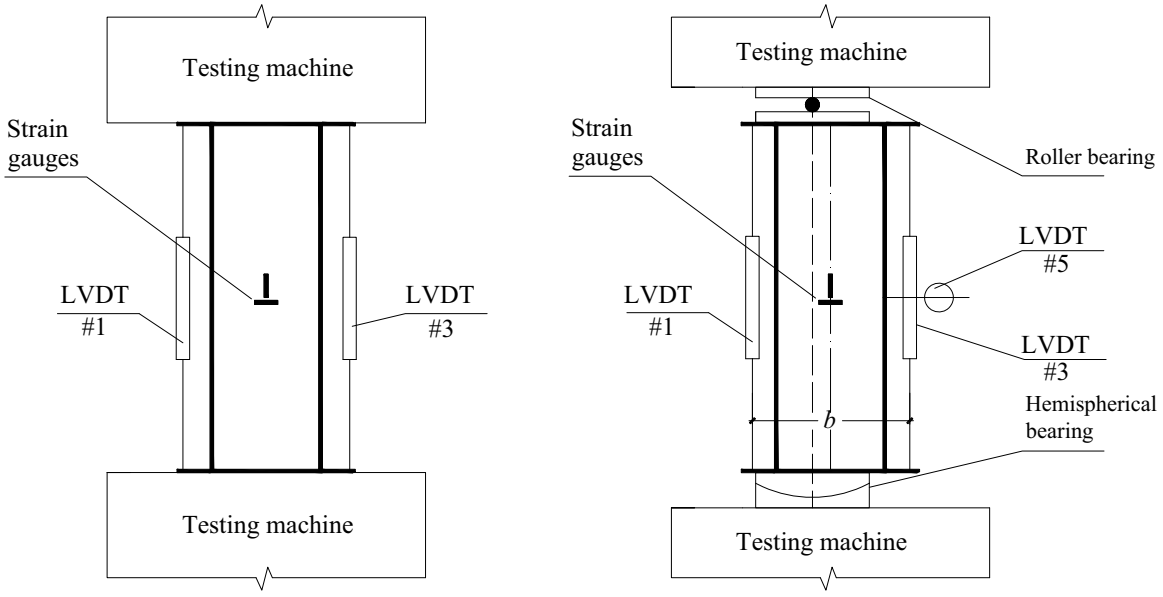

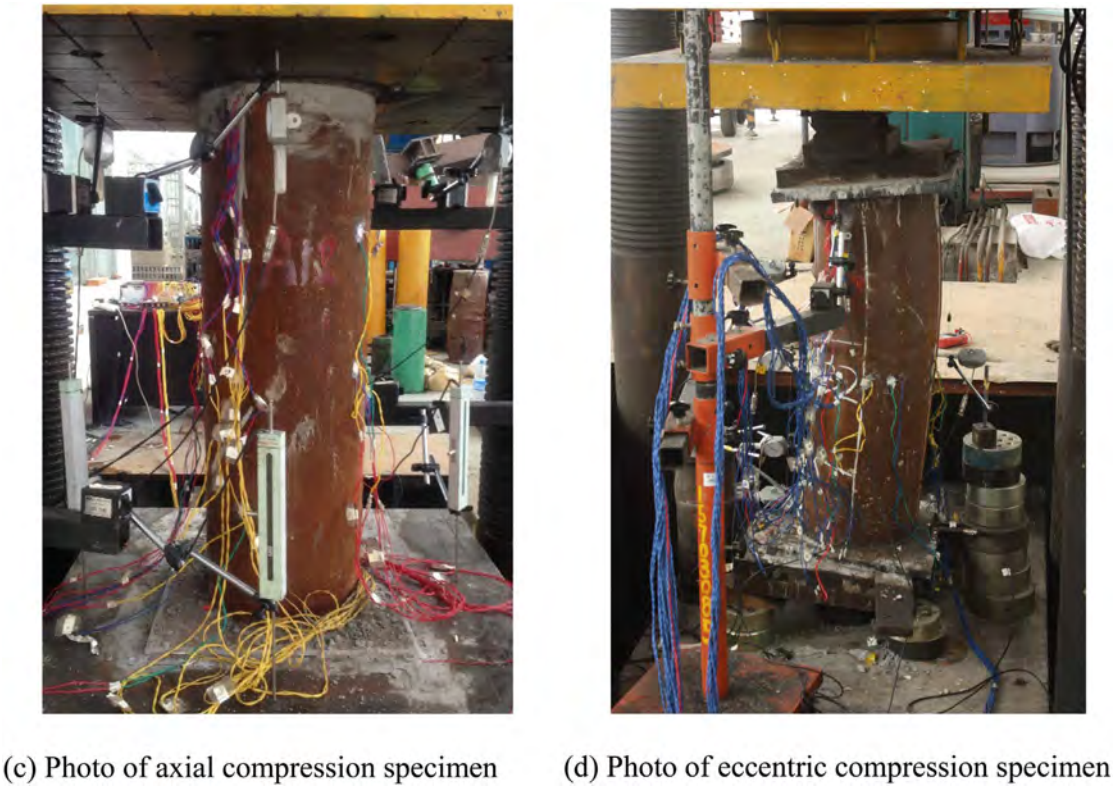

Fig. 3. Test set-up and instrumentation. (a) Axial compression (b) Eccentric compression (c) Photo of axial compression specimen (d) Photo of eccentric compression specimen.

steel jacketing specimens BZ1–BZ5 under axial loading. Fig. 6 shows the typical experimental load-curvature response of specimens BZ11 and CZ9 under eccentric loading. It can be seen that the columns behaved elastically at the early stage of loading. The deformations increased linearly with the increase of loads. When the load reached approximate 60% of the maximum load, the curves showed elasto-plastic behaviour, which coincide the experimental observation that the shear slip lines appeared. After the peak strength was attained, the axial load on no-retrofitted specimen AZ1 descended dramatically while the retrofitted columns exhibited ductile behaviour as the load remained constant or decreased slightly. In addition, as shown in Fig. 5, the strains corresponding to the peak load of specimens BZ1–BZ5 are 3040 με, 5600 με, 7100 με, 8300 με and 8750 με respectively, which implied that the deformation capacity of the column rises as the thickness of the steel tube increases.

Fig. 4. Experimental observations and failure modes. (a) Shear slip lines under axial compression (b) Dilation of steel tube (c) Shear slip lines under eccentric compression (d) Local buckling of steel tube.

3.3. *Effect of axial preloading*

Fig. 7 shows the influence of change in axial preloading level for the specimens under axial compression. It can be seen that the effects of preloads on the axial compression strength and deformation capacity were negligible. As the axial preloading level increased from 0.4 to 0.5, the ultimate strength of the retrofitted column slightly decreased from 96.2–94.8%, and the strain corresponding to the peak strength reduced from 88.6–85.2%.

The effect of axial preloading for the specimens subjected to eccentric compression is shown in Fig. 8. The relative compressive strength factor α defined as the ratio of the eccentric compressive strength versus the axial compressive strength of the column obtained from the experimental test. As depicted in Fig. 8, the eccentric compressive strength of the columns decreased after preloading. For example, for the columns with 2 mm thick steel tube, the strength of specimen CZ4 was 14.1% lower than that of specimen BZ7 with the effect of level 0.08 of axial preloading, given that the imposed loads

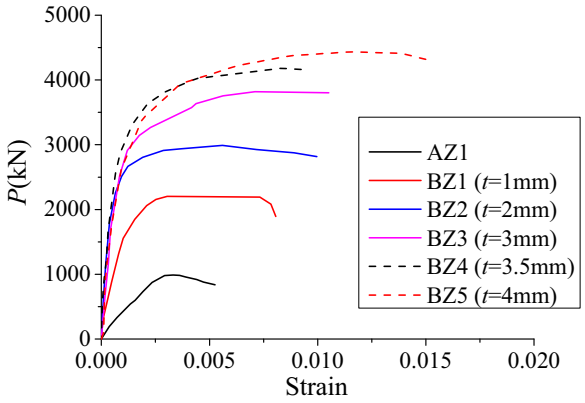

Fig. 5. Load (P) versus average longitudinal strain curves under axial compression.

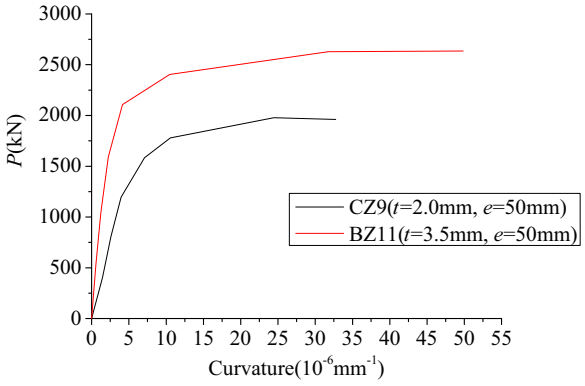

Fig. 6. Load (P) versus curvature curves under eccentric compression.

on the retrofitted columns have same eccentricity 30 mm. However, the influence of change in axial preloading level on the ultimate strength of column reduced as the thickness of steel tube increased. For the columns with 3.5 mm thick steel tube, the maximum percentage difference between the non-preloaded and preloaded (level 0.08 of axial preloading) specimens on eccentric compressive strength reduced to 9.6%. When the thickness of the steel tube is 4 mm, the effect of preload was barely significant.

3.4. Strains distributions

Fig. 9 shows the development of transverse strains around the circumference of steel tube under loading. The strain measurement points are located at the mid-height of the specimens.

It can be observed that the transverse strains developed elastically until about 70% of the maximum loads. After that, the strains increased rapidly and approached yield strain limit at the peak load. It demonstrated that the steel jacket could provide sufficient confinement on the core concrete. Fig. 10 shows the longitudinal strain distribution of steel tubes. As can be seen, the longitudinal strain distributions maintain linear through the cross-section prior to the maximum load. Thus the plane section assumption in analysis can be applicable to the steel-jacket retrofitted RC columns.

4. Numerical modelling

4.1. Fibre element model considering preload effect

A fibre element model was developed using OpenSees to investigate the nonlinear behaviour of steel-jacket retrofitted RC columns with preload effects. In the fibre element model, the column was divided into four NonlinerBeamColumn elements along the member length. The column section in each element was further discretised into a cluster of fibres as showed in Fig. 11. The concrete part was discretised by 200 mm × 200 mm size fibres and the steel part was divided into four layers in radial direction and thirty-six fibres in each layer. Each fibre element represents a fibre of material deforming longitudinally along the member and can be assigned specific material properties. The fibre stresses were calculated from the fibre strains using assigned uniaxial stress-strain relations incorporating the confining effects if necessary. In order to simulate the effect of preloading, the initial strains were applied on the fibres of the original columns to ensure the resultant forces of the applied stresses agreed well with the actual preload actions. For application of boundary condition, as shown in Fig. 11, the translational displacements in the X and Y directions were restrained in Node2 while the translational displacements in the X, Y and Z directions were restrained in Node1. The additional external loads were imposed by a concentrated force P_f on the top of the column and a pair of bending moment M_f at both support ends.

4.2. Modelling of concrete material

The elastio-plastic uniaxial material model Concrete02 provided by the material library of OpenSees was adopted for the concrete in original columns and the infill concrete between

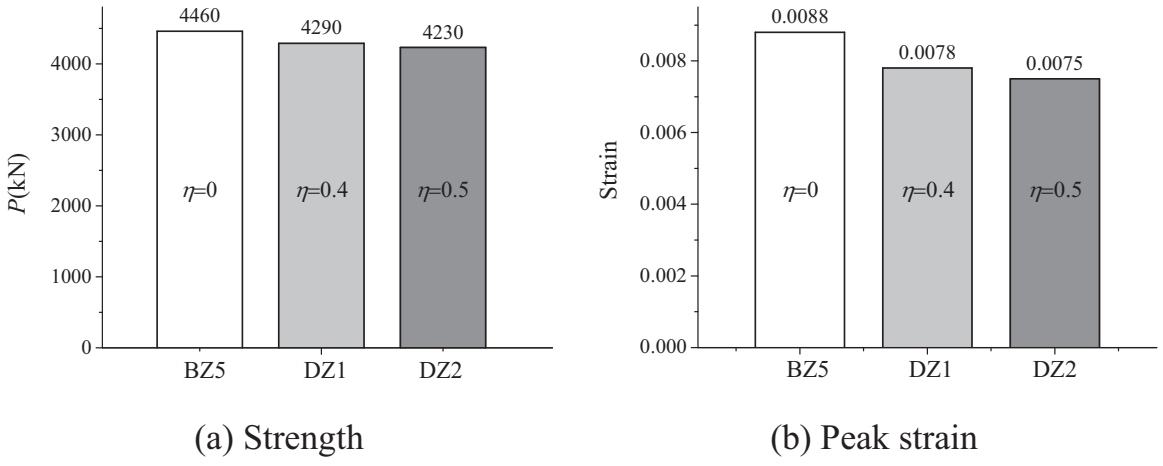

Fig. 7. Effect of axial preloading level on axial compressive behaviour. (a) Strength (b) Peak strain.

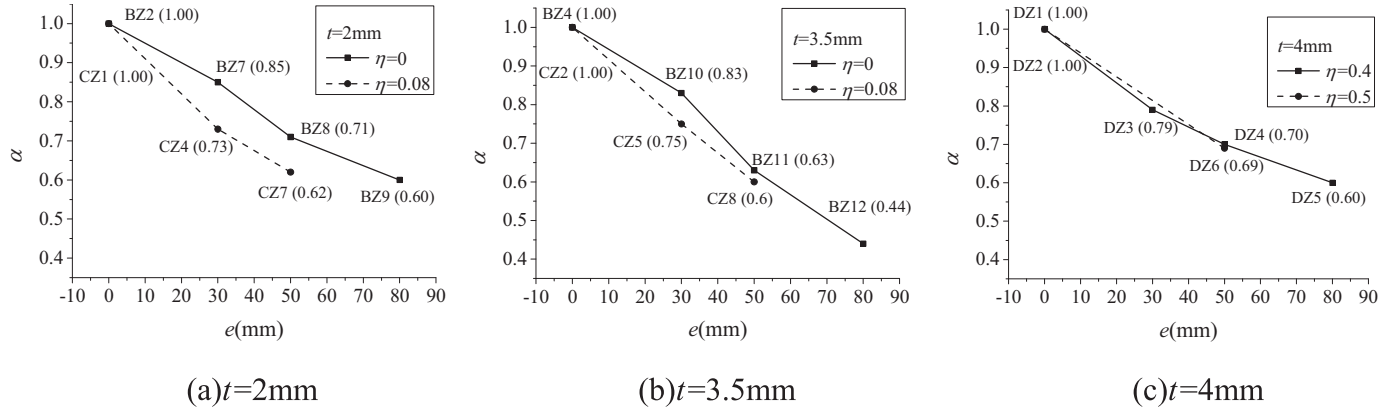

Fig. 8. Effect of axial preloading level on eccentric compressive strength. (a)t=2 mm (b)t=3.5 mm (c)t=4 mm.

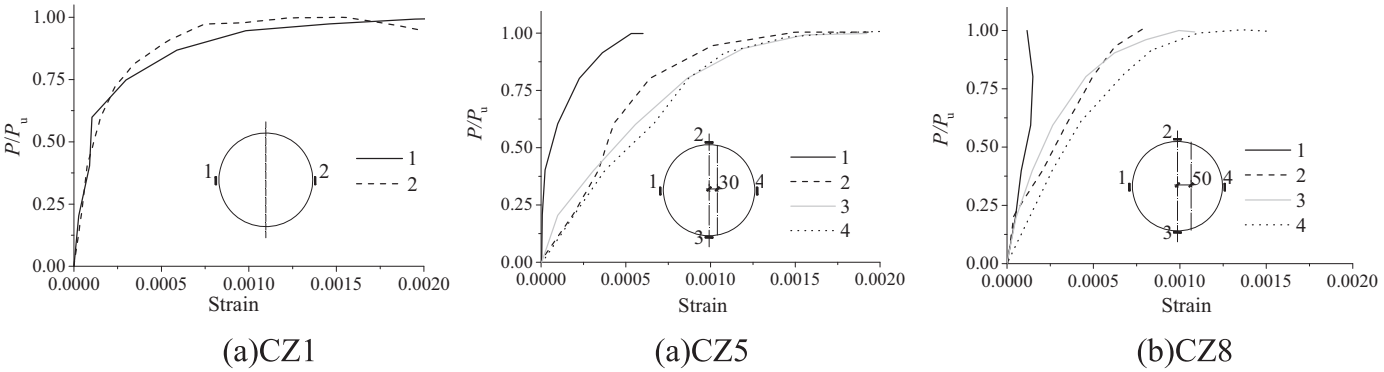

Fig. 9. P/P_u versus transverse strains of steel tubes. (a)CZ1 (a)CZ5 (b)CZ8.

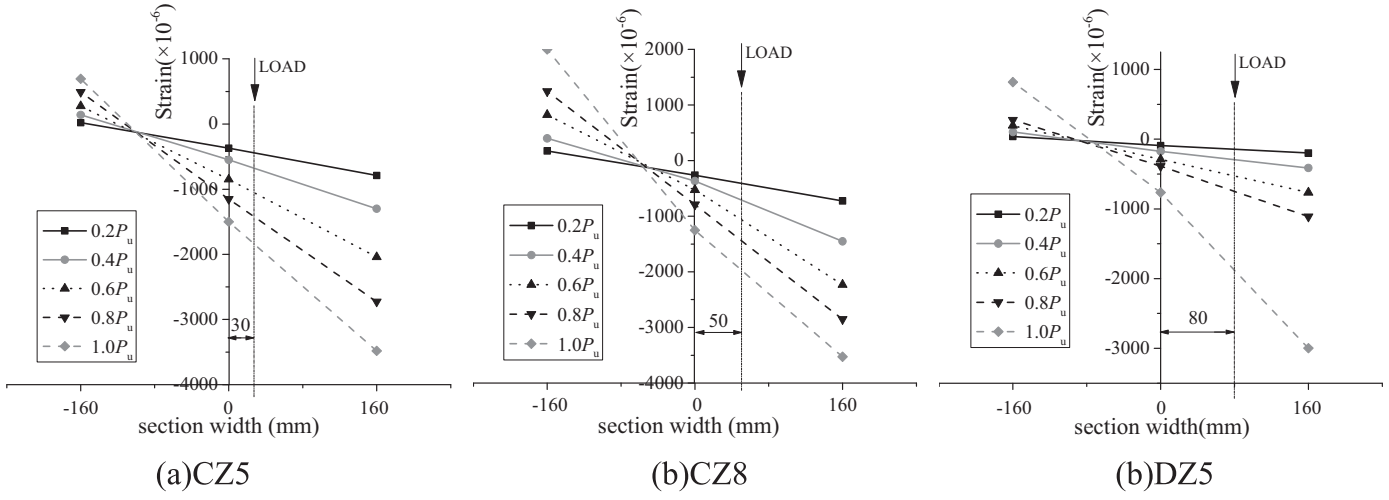

Fig. 10. Longitudinal strain distributions of steel tubes. (a)CZ5 (b)CZ8 (b)DZ5.

original column and steel tube. The typical stress-strain curve is shown in Fig. 12. In this model, f_{cc} and ε_{cc} are the axial peak stress and the corresponding strain; f_{cu} and ε_{cu} are the crushing strength and the corresponding strain; f_t is the tensile strength that is taken as $0.3(f_c)^{2/3}$ [16]; E_{ts} is the tension softening stiffness that is chosen to be 4000 MPa in this study.

Compared with the conventional RC column and the normal concrete-filled steel tube (CFST) column, the steel-jacket retrofitted column contains two types of concrete with different strengths inside the steel jacket. The concretes are in tri-axial compressive stress state when the column subjected to compressive loading. The confinement effects of the steel jacket on the concretes are significant and should be taken into consideration, but also the stirrup of the original column would provide extra lateral constraint force on the core concrete and their confinement effects could not be neglected. In the following sections, a simplified mechanical model is presented to determine the value of f_{cc}, ε_{cc}, f_{cu} and ε_{cu} for the original core concrete and infill concrete incorporating the confining effects.

4.2.1. *Confining stresses*

The confining stress state of the core concrete is shown in Fig. 13. The confinement effects on the core concrete can be divided into two parts. The first part of the confining pressure (f_{l1}) is imposed by the steel tube, which is assumed to be linear distribution across the whole section, as is shown in Fig. 13(a). The

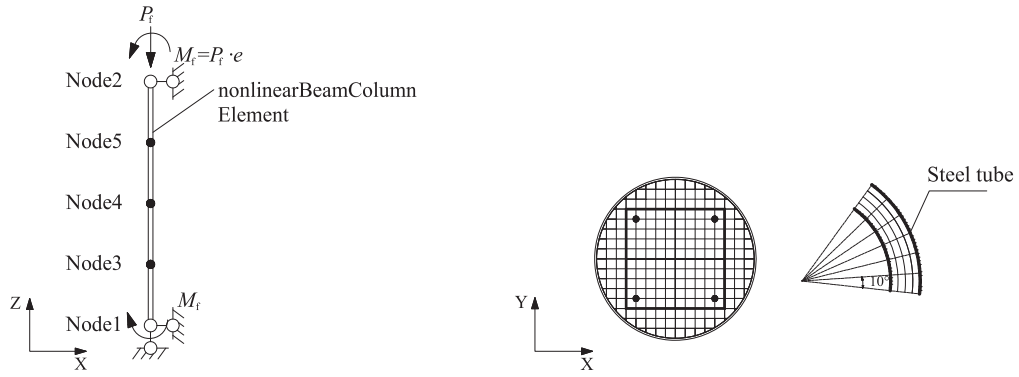

(a) Node, element and boundary condition

(b) Section discretization of concrete and steel tube

Fig. 11. Details of FEA model. (a) Node, element and boundary condition (b) Section discretization of concrete and steel tube.

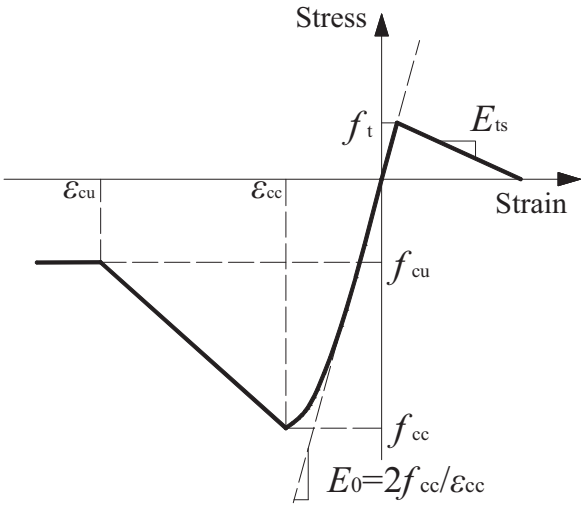

Fig. 12. Stress-strain model for Concrete02 in OpenSees.

second part of the confining pressure (f_{l2}) is caused by the stirrup of the original column, and is assumed to be applied on the effective confined core of the original column, as is depicted in Fig. 13(b). Thus, the confining pressures on the original core concrete and infill concrete are taken from $f_{l1}+f_{l2}$ and f_{l1} respectively.

4.2.2. Determination of f_{l1}

Based on the equilibrium state as illustrated in Fig. 13(a), the lateral confining pressure f_{l1} from the steel jacket can be obtained from

$$2f_{sh1}t = f_{l1}(D - 2t) \tag{1}$$

which is re-written as

$$f_{l1} = \frac{2f_{sh1}t}{D - 2t} \tag{2}$$

where f_{sh1} is the loop stress of the steel jacket that is given [17] by

$$f_{sh1} = 0.19f_y \quad (\text{for } 16.7 < D/t < 152) \tag{3}$$

in which f_y is the yield strength of steel tube. The effective lateral confining pressure f'_{l1} can be calculated by

$$f'_{l1} = k_{e1}f_{l1} \tag{4}$$

where k_{e1} is the confinement effectiveness coefficient and is taken as 1.0 for the concrete filled steel tube components.

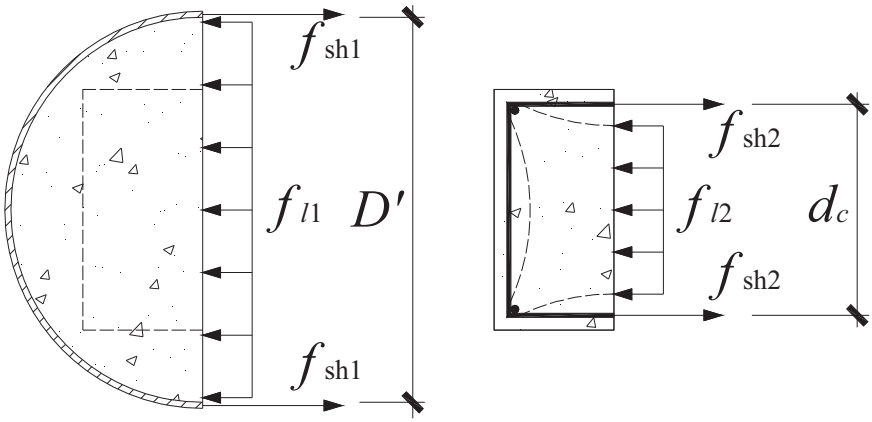

(a) f_{l1} (b) f_{l2}

Fig. 13. Confining pressure of infill concrete and original concrete. (a) f_{l1} (b) f_{l2}.

4.2.3. Determination of f_{l2}

As proposed by Mander *et al.* [18] and following the equilibrium state shown in Fig. 13(b), the effective lateral confining pressure f'_{l2} from the stirrup is given by

$$f'_{l2} = k_{e2} f_{l2} \tag{5}$$

where

$$f_{l2} = \frac{2f_{sh2}A'_{s2}}{sd_c} \tag{6}$$

$$k_{e2} = \frac{\left(1 - 4.\frac{w^2}{6d_c^2}\right)\left(1 - \frac{s'}{2d_c}\right)^2}{(1 - \rho_{cc})} \tag{7}$$

in which f_{sh2} is the yield strength of transverse reinforcement, A'_{s2} the area of transverse reinforcement bar, s the centre to centre spacing of spirals, d_c the diameter of spiral bars, w the clear distance between adjacent longitudinal bars, s' the clear vertical spacing between spiral bars, ρ_{cc} the ratio of area of longitudinal reinforcement to area of core of section.

4.2.4. Determination of f_{cc}

To determine the confined concrete compressive strength f_{cc}, the failure criterion proposed by Guo *et al.* [19] which includes a specified ultimate strength surface for multiaxial compressive stresses is used in this model. For the doubly symmetric cross-section, the equations can be simplified as

$$\tau_0 = 6.9638\left(\frac{0.09 - \sigma_0}{c - \sigma_0}\right)^{0.9297} \tag{8}$$

$$c = 12.2445(\cos 1.5\alpha)^{1.5} + 7.3319(\sin 1.5\alpha)^2 \tag{9}$$

$$\sigma_0 = \frac{\sigma_{oct}}{f_c},\ \tau_0 = \frac{\tau_{oct}}{f_c} \tag{10}$$

$$\sigma_{oct} = \frac{2f' + f_{cc}}{3} \tag{11}$$

$$\tau_{oct} = \frac{\sqrt{2(f' - f_{cc})^2}}{3} \tag{12}$$

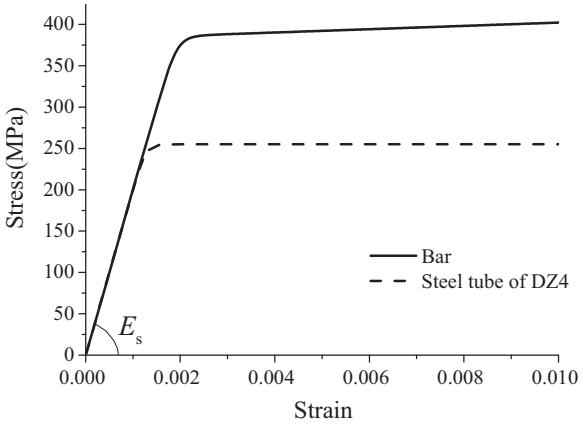

Fig. 14. Stress-strain relationship of steel.

$$\cos\alpha = \frac{f' - f_{cc}}{3\sqrt{2}\,\tau_{oct}} \tag{13}$$

where σ_{oct} and τ_{oct} are the normal and shear octahedral stresses, respectively; the rotational variable α defines the direction of deviatoric components on the octahedral plane; f' is the effective lateral confining stresses on the concretes. For the original concrete, f' is taken as $f'_{l1}+f'_{l2}$. For the infill concrete, f' is taken as f'_{l1}.

4.2.5. Determination of ε_{cc}

The strain ε_{cc} corresponding to f_{cc} is determined as [18]

$$\varepsilon_{cc} = \varepsilon_{c0}\left[1 + k_2\frac{f'}{f_{c0}}\right] \tag{14}$$

where k_2 is taken as 20.5 [20]; f_{c0} is the maximum compressive stress of unconfined concrete and ε_{c0} is its corresponding strain which can be calculated [21] by

$$\varepsilon_{c0} = \left(700 + 172\sqrt{f_{c0}}\right) \times 10^{-6}. \tag{15}$$

4.2.6. Determination of f_{cu} and ε_{cu}

As suggested by Hu *et al.* [22] the ultimate strength f_{cu} and its corresponding strain ε_{cu}, are given by

$$f_{cu} = \beta_c f_{cc} \tag{16}$$

$$\beta_c = \begin{cases} 1.0 & D/t \le 40 \\ 0.0000339\left(\frac{D}{t}\right)^2 - 0.010085\left(\frac{D}{t}\right) + 1.3491 & 40 < D/t \le 150 \end{cases} \tag{17}$$

$$\varepsilon_{cu} = 11\varepsilon_{cc} \tag{18}$$

4.3. Modelling of steel material

The elastio-plastic uniaxial material model Steel02 provided by the material library of OpenSees was used for all the steel components. As can be seen in Fig. 14 shows, the elasticity modulus E_s is taken as 200 GPa. The strain-hardening effect of the steel jacket is neglected because local buckling occurred when the specimens almost attain its peak strengths. For the steel bars which are constrained by the external concrete, the strain-hardening ratio is taken as $0.001E_s$. The yield stress values of the steel components are listed from Table 2.

4.4. Validation

In order to validate the proposed numerical model, the results predicted by the fibre element model were compared with the experimental results reported herein and in other literature [23]. Fig. 15 shows some comparison examples of the axial load-strain curves. Fig. 16 shows the curves of applied load versus lateral displacement at the mid-height for the specimens under eccentric compressive loads while the applied load versus curvature curves are depicted in Fig. 17. It can be seen that the results obtained from the proposed method are in good agreement with the experimental results. Table 3 lists the maximum experimental loads P_u of the columns compared with the ones P_{FE} predicted by the proposed model. The mean value of P_{FE}/P_u is 0.982 with the COV of 0.079. It can be concluded that the fibre element model could accurately predict the ultimate strength and load-deflection behaviour of the steel-jacket retrofitted columns with preload effects under concentric and eccentric compression.

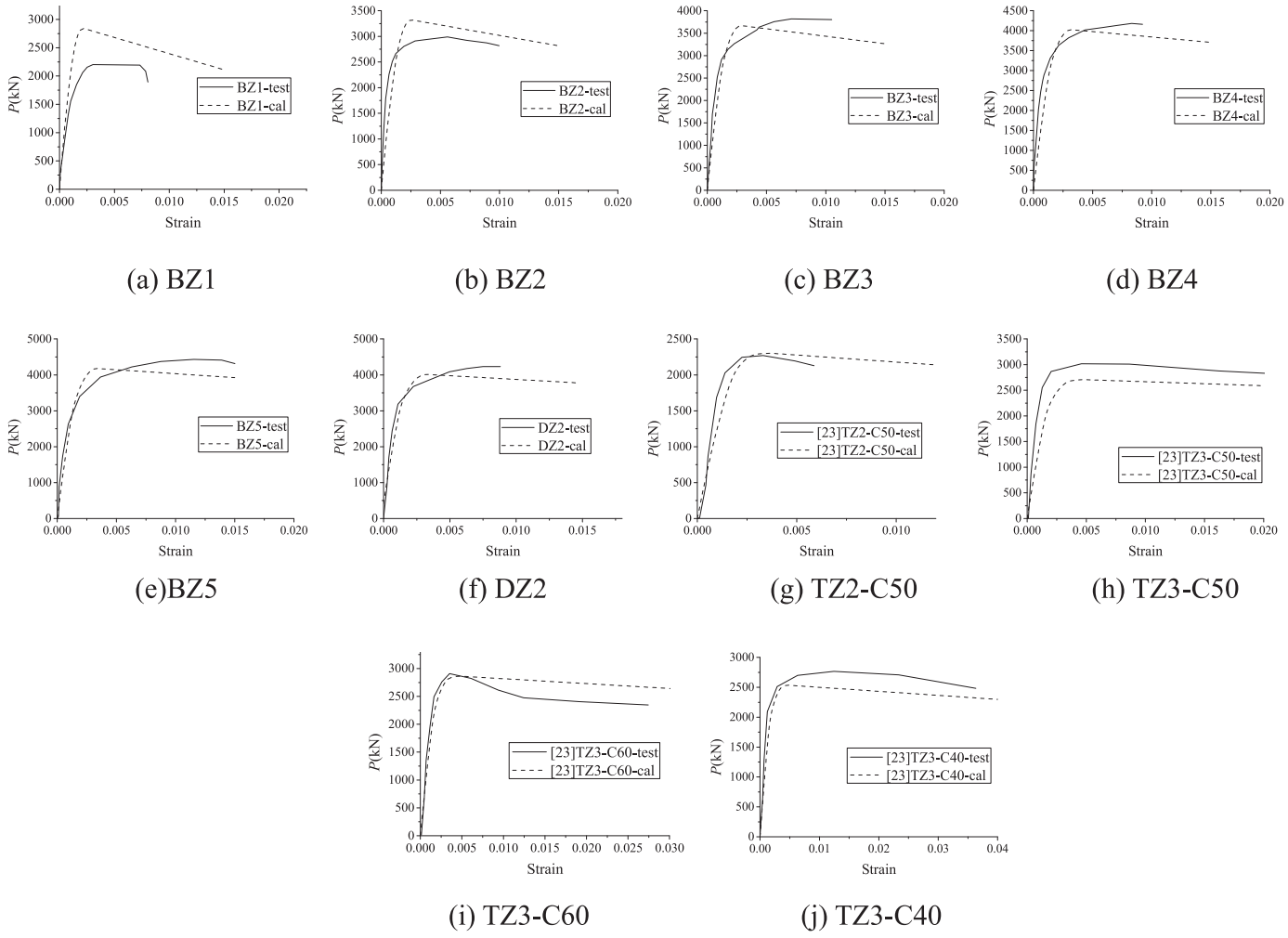

Fig. 15. Comparisons of axial load-deflection curves. (a) BZ1 (b) BZ2 (c) BZ3 (d) BZ4 (e)BZ5 (f) DZ2 (g) TZ2-C50 (h) TZ3-C50 (i) TZ3-C60 (j) TZ3-C40.

The experimental results were also compared with the results calculated by the methods in current design codes CECS 28–2012 [24], ANSI/AISC-360–2005 [25], EC4 [26] and AIJ-CFT [27]. The comparison results are shown in Table 3. It should be noted that the currently preload effects are not included in any design code. It is observed that the design code CECS 28–2012 (P_{CECS}) gives the most accurate predictions among all of them. The mean value and COV of P_{CECS}/P_u are 1.062 and 0.088 respectively. The other design codes apparently underestimate the ultimate strength of the columns.

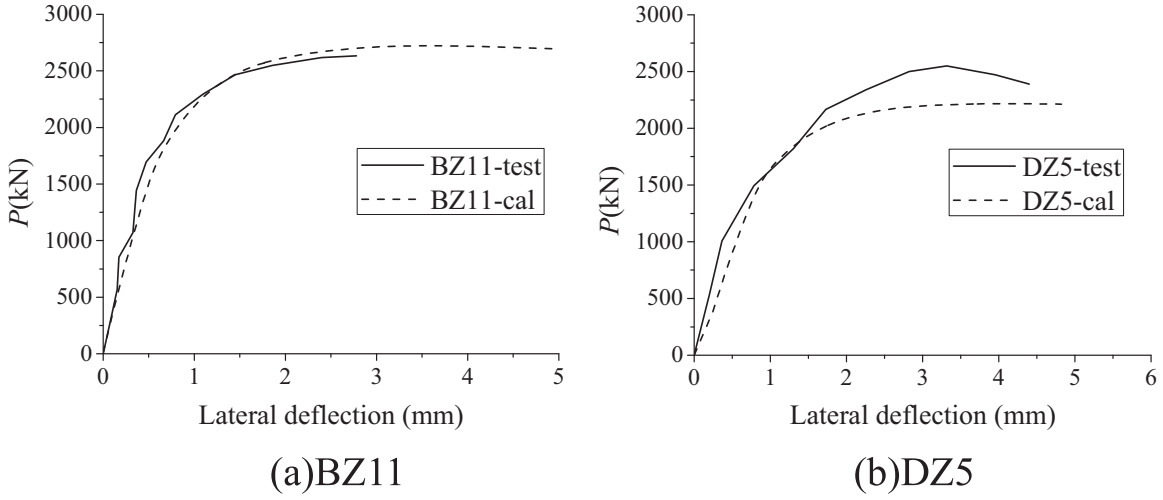

Fig. 16. Comparisons of eccentric load versus lateral deflection curves. (a)BZ11 (b)DZ5.

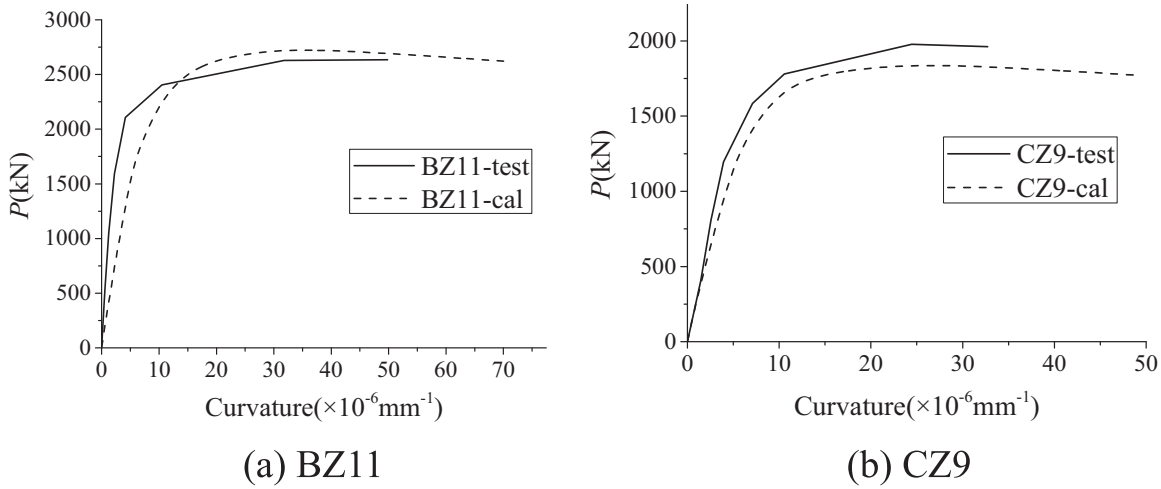

Fig. 17. Comparisons of eccentric load versus curvature curves. (a) BZ11 (b) CZ9.

5. Effects of preloading

5.1. Effects of axial and moment preloading

Depended on the structural system, the preloading actions on the original core concrete may be in form of axial compression with or without bending moment. In order to further investigate the effect of preloading on the ultimate strength of retrofitted column, columns under seven combinations of axial and moment preloads together with a non-preloaded one are considered. The columns have identical dimensions and material properties as specimen DZ2. Details of seven preload combinations named as PS1–PS7 are shown in Fig. 18. It is noted that the preload actions are selected based on the bending-axial load interaction curve of the original RC column. Some of the preload actions might tend to cause the column failing in tension and some in compression. The magnitudes of selected preload actions are close to but below the ultimate load-bearing capacities of the original column. The retrofitted column with a specific preload combination is additionally loaded under compressive forces with varied eccentricity to obtain its axial load-bending moment (*P-M*) interaction strength curve. Fig. 18 also shows the obtained example *P-M* interaction strength curve for the column with preload combination PS3. The positive value of moment in the interaction curve denotes that the applied bending moment is imposed in the same direction as the moment preload while the negative value denotes the opposite direction. The *P-M* interaction strength curves for all the columns with different preload combinations and non-preload case (PS0) are shown in Fig. 19. It can be seen that the *P-M* interaction strength curves for all the columns are similar, but the effect of preload could be apparently observed and might increase or decrease the strength of the retrofitted column.

In order to quantitatively evaluate the effects of preloads, four preload effect indexes indicating the differences between the non-preloaded and preloaded column: (1) reduction of axial compressive strength ΔP_{max}, (2) reduction of minimum bending moment ΔM_{min}, (3) reduction of axial force in compression-controlled failure area ΔP and (4) reduction of bending moment in compression-controlled failure area ΔM, are introduced as shown in Fig. 19. The preload effect indexes of the columns having different preload combinations are compared and presented in Fig. 20, in which $P_{max,\ PS0}$ is the axial compressive strength of column without preloads, $M_{max,\ PS0}$ is the maximum flexural strength in *P-M* interaction strength curve without preloads. It is shown that the preloads that are more susceptible to causing flexure failure of original column might have more adverse effect on the strength of retrofitted columns. In this example, the preload combination PS2 is the most unfavourable one. On the other hand, the preload combinations with high axial load levels such as PS6 and PS7 could produce positive effects on the strength of the columns.

5.2. Effects of preloads and other parameters

The *P-M* interaction strength curves of steel-jacketing retrofitted columns could be influenced by other parameters including the D/t ratio, the steel yield strengths of steel tube f_y, the strength of infill concrete f_{c2} and area enlargement factor β (the ratio of the cross-sectional area of infill concrete to the cross-sectional area of original concrete.) The effects of preloads and other parameters on *P-M* interaction strength curves of retrofitted columns are shown in Fig. 21. Only the most adverse preload case PS2 is taken into account herein to compare with the non-preload case PS0. Fig. 22 shows the comparison of the preload effect indexes of the columns with different D/t, f_y, f_{c2} and β. As can be seen, the effects of preloads become less adverse when the D/t ratios decrease or the yield strengths of steel tube increase. The effects of preloads are marginally influenced by the change in the strength of infill concrete and area enlargement factor.

6. Conclusions

Experimental and numerical studies on the behaviour of steel-jacket retrofitted RC columns with preload effects were performed. Twenty-nine columns retrofitted by steel jackets were tested under concentrically or eccentrically compressive loading. The experimental results manifested that the effects of axial preloading on the axial compressive strength of retrofitted columns are negligible. The observation is in consistent with the previous research finding of Takeuti *et al.* [12] on concrete jacketed columns. The eccentric compressive strength of the columns decreased after preloading, but the influence reduced as the thickness of steel tube increased. A fibre element model is developed to predict the behaviour of the retrofitted columns. The geometric and material non-linear behaviour of all the components, the steel tube and stirrup confining effects on the concretes and the preloading actions are taken into account in the model. The ultimate strengths and load-deflection curves of the columns predicted by the proposed numerical model were compared with the experimental results and both results are in good agreement. The experimental results were also compared with the results calculated by the

Table 3
Comparisons of test results and results predicted by design codes and proposed model.

Source	Specimen	Test result	CECS 28-2012		ANSI/AISC-360–2005		EC4		AIJ-CFT		Proposed model	
		P_u (kN)	P_{CECS} (kN)	P_{CECS}/P_u	P_{ANSI} (kN)	P_{ANSI}/P_u	P_{EC4} (kN)	P_{EC4}/P_u	P_{AIJ} (kN)	P_{AIJ}/P_u	P_{FE} (kN)	P_{FE}/P_u
This paper	BZ1	2202	2945	–	2500	–	2951	–	2332	–	2842	–
	BZ2	2990	3553	1.188	2804	0.938	3409	1.140	2780	0.930	3320	1.110
	BZ3	3820	4007	1.049	3032	0.794	3761	0.984	3055	0.800	3668	0.960
	BZ4	4180	4477	1.071	3266	0.781	4114	0.984	3328	0.796	4025	0.963
	BZ5	4460	4684	1.050	3370	0.756	4277	0.959	3460	0.776	4180	0.937
	BZ6	Early failure due to weld fracture										
	BZ7	2540	2638	1.039	1058	0.417	1922	0.757	2020	0.795	2550	1.004
	BZ8	2108	2251	1.068	792	0.376	1536	0.729	1753	0.832	2180	1.034
	BZ9	1797	1846	1.027	576	0.321	1180	0.657	1405	0.782	1704	0.948
	BZ10	3450	3324	0.963	1472	0.427	2480	0.719	2338	0.678	3137	0.909
	BZ11	2636	2837	1.076	1166	0.442	1961	0.744	2056	0.780	2721	1.032
	BZ12	1850	2326	1.257	884	0.478	1483	0.802	1699	0.918	2177	1.177
	CZ1	2780	2978	1.071	2324	0.836	2847	1.024	2257	0.812	2770	0.996
	CZ2	3678	4057	1.103	2862	0.778	3672	0.998	3005	0.817	3585	0.975
	CZ3	3030	2978	0.983	2324	0.767	2847	0.940	2257	0.745	2770	0.914
	CZ4	2040	2211	1.084	908	0.445	1598	0.783	1651	0.809	2137	1.048
	CZ5	2741	3012	1.099	1362	0.497	2229	0.813	2033	0.742	2808	1.024
	CZ6	2988	3012	1.008	1362	0.456	2229	0.746	2033	0.680	2807	0.939
	CZ7	1727	1887	1.093	688	0.398	1273	0.737	1439	0.833	1836	1.063
	CZ8	2190	2571	1.174	1094	0.500	1790	0.817	1801	0.822	2447	1.117
	CZ9	1980	2571	1.298	688	0.347	1273	0.643	1439	0.727	1836	0.927
	CZ10	2136	2571	1.204	1094	0.512	1790	0.838	1801	0.843	2447	1.146
	DZ1	4290	4521	1.054	3235	0.754	4121	0.961	3334	0.777	4021	0.937
	DZ2	4230	4521	1.069	3235	0.765	4121	0.974	3334	0.788	4019	0.950
	DZ3	3380	3357	0.993	1504	0.445	2502	0.740	2305	0.682	3157	0.934
	DZ4	3000	2865	0.955	1200	0.400	1992	0.664	2029	0.676	2745	0.915
	DZ5	2560	2349	0.917	922	0.360	1498	0.585	1683	0.658	2212	0.864
	DZ6	2920	2865	0.981	1200	0.411	1992	0.682	2029	0.695	2744	0.940
[23]	TZ3-C50	3029	2935	0.969	1989	0.657	3029	0.855	1973	0.651	2707	0.894
	TZ2-C50	2265	2381	1.051	1726	0.762	2265	0.963	1782	0.787	2300	1.015
	TZ4-C50	3274	3169	0.968	2100	0.641	3274	0.844	2270	0.693	2875	0.878
	TZ3-C40	2768	2812	1.016	1885	0.681	2768	0.901	1869	0.675	2534	0.915
	TZ3-C60	2914	3046	1.045	2083	0.715	2914	0.921	2067	0.709	2862	0.982
Mean	All specimens expect[23]			1.072		0.554		0.824		0.777		0.991
COV				0.092		0.188		0.143		0.071		0.080
Mean	[23]			1.010		0.691		0.897		0.703		0.937
COV				0.040		0.048		0.049		0.052		0.059
Mean	All specimens			1.062		0.576		0.836		0.765		0.982
COV				0.088		0.180		0.135		0.073		0.079

Note: The D/t ratio of specimen BZ1 is 320 whose value is out of applicable range of the proposed model. Thus, the results of specimen BZ1 are not included in comparison.

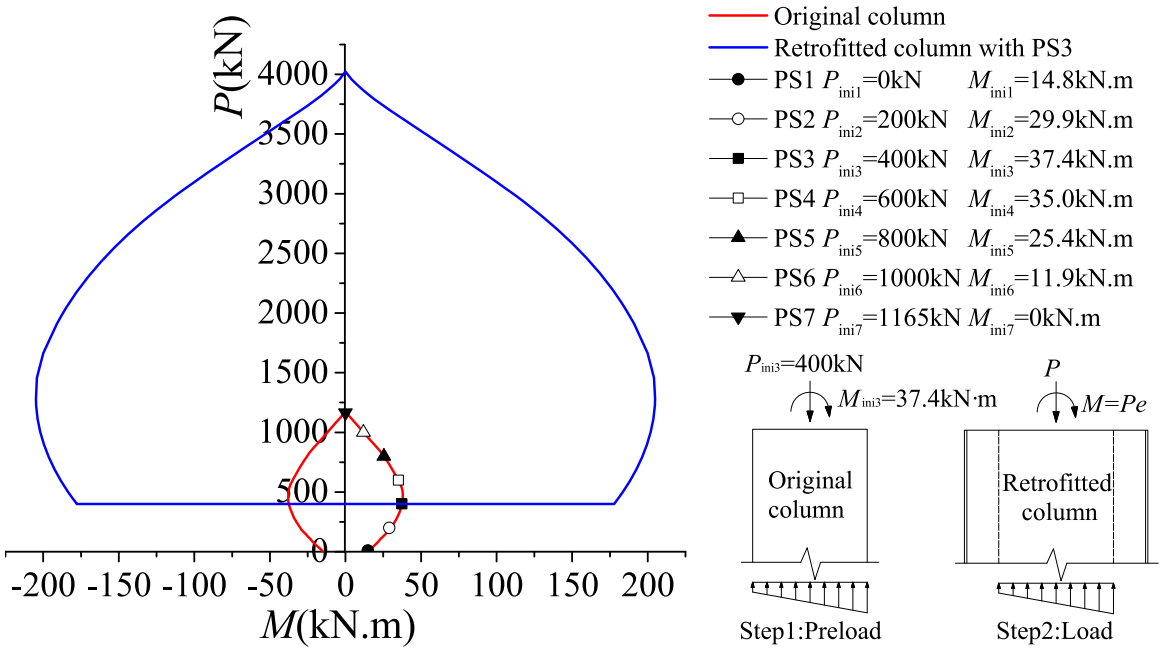

Fig. 18. Selected preload combinations and example *P-M* interaction strength curve.

methods in current design codes and indicated that the design code CECS 28–2012 gave the most accurate predictions. Further parametric evaluations of the effect of preloading using quantitative factors were undertaken. The effects of axial and moment preloading on the strength of retrofitted column and the effects of preloads with various other parameters including the diameter-to-thickness ratio, strength of steel tube, strength of infill concrete and the area enlargement were investigated. It was found that the axial and moment preload combinations that were more susceptible to causing flexure failure of the original column might have more adverse effect on the ultimate strength of retrofitted columns. The effects of preload became less adverse when the D/t ratios decreased or the yield strengths of steel tube increased while the influences of change in the strength of infill concrete and area enlargement on the effect of preloading were barely significant.

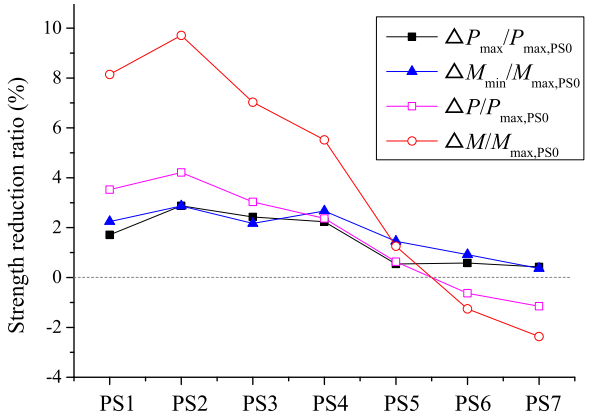

Fig. 20. Comparisons of preload effect indexes of columns with different preload combinations.

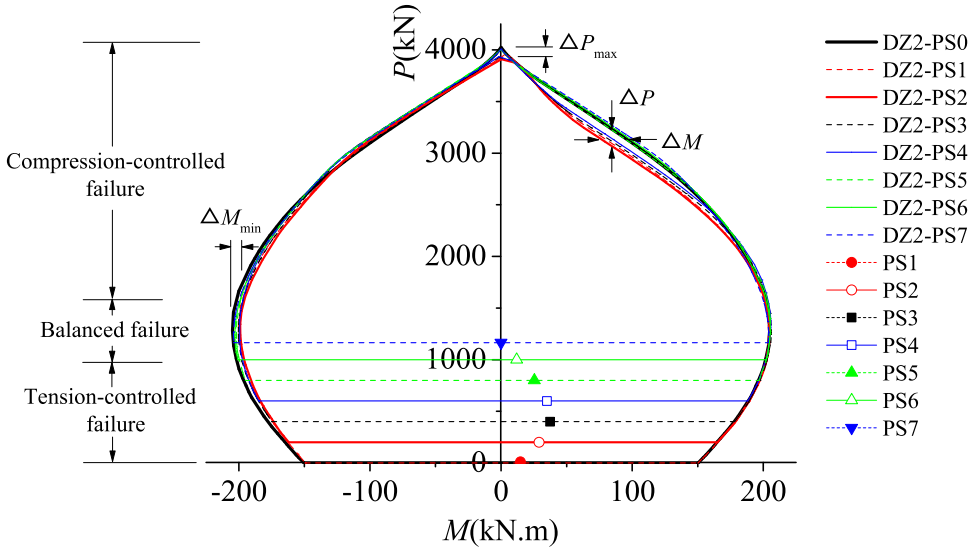

Fig. 19. Effects of axial and moment preloading on *P-M* interaction strength curves.

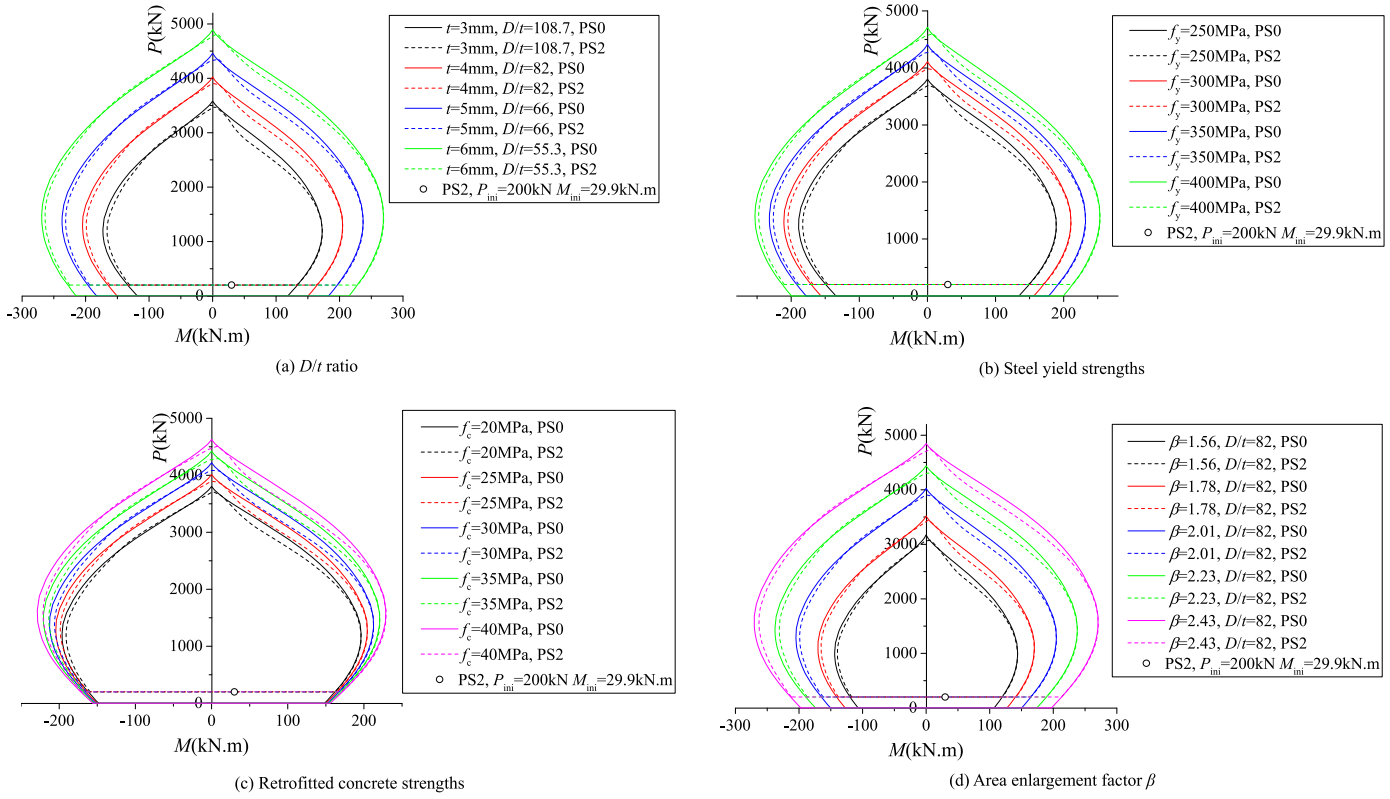

Fig. 21. Effects of preloads and other parameters on *P-M* interaction strength curves. (a) *D*/*t* ratio (b) Steel yield strengths (c) Retrofitted concrete strengths (d) Area enlargement factor β.

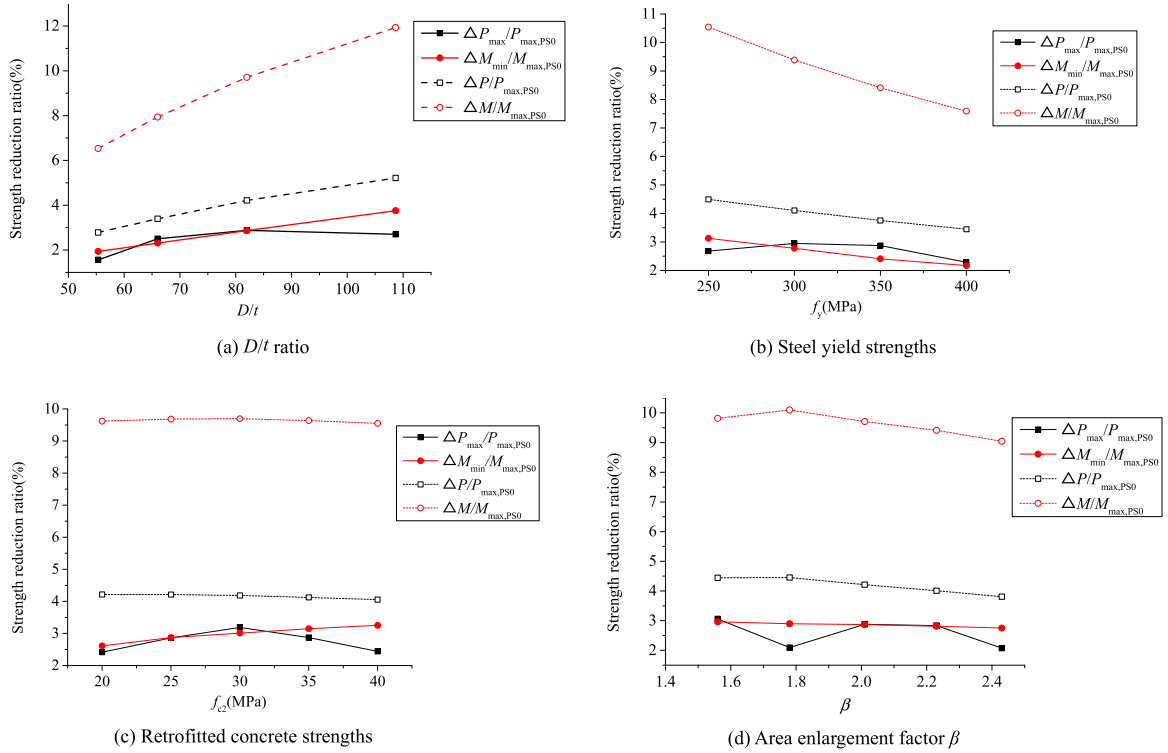

Fig. 22. Comparisons of preload effect indexes of columns considering different parameters. (a) *D*/*t* ratio (b) Steel yield strengths (c) Retrofitted concrete strengths (d) Area enlargement factor β.

Acknowledgements

Funding for this research project was provided by the China Scholarship Council, the Fundamental Research Funds for the Central Universities (2014ZZ0026), the State Key Lab of Subtropical Building Science, South China University of Technology (Project No. 2015ZC18), the National Natural Science Foundation of China (51578246). The supports for the research are acknowledged with thanks.

References

[1] H. Sezen, E. Miller, Experimental evaluation of axial behavior of strengthened circular reinforced-concrete columns, J. Bridge Eng. 16 (2) (2011) 238–247.
[2] Y.H. Chai, M.J.N. Priestley, F. Seible, Seismic retrofit of circular bridge columns for enhanced flexural performance, ACI Struct. J. 88 (5) (1991) 572–584.
[3] Y.H. Chai, An analysis of the seismic characteristics of steel-jacketed circular bridge columns, Earthq. Eng. Struct. Dyn. 25 (2) (1996) 149–161.
[4] M.J.N. Priestley, F. Seible, Y. Xiao, R. Verma, Steel jacket retrofitting of reinforced concrete bridge columns for enhanced shear strength-part 1: theoretical considerations and test design, ACI Struct. J. 91 (5) (1994) 394–405.
[5] M.J.N. Priestley, F. Seible, Y. Xiao, Steel jacket retrofitting of reinforced concrete bridge columns for enhanced shear strength-part 2: test results and comparison with theory, ACI Struct. J. 91 (5) (1994) 537–551.
[6] Y. Xiao, R. Ma, Seismic retrofit of RC circular columns using prefabricated composite jacketing, J. Struct. Eng. 123 (10) (1997) 1357–1364.
[7] Y. Xiao, H. Wu, Retrofit of reinforced concrete columns using partially stiffened steel jackets, J. Struct. Eng. 129 (6) (2003) 725–732.
[8] Y.F. Li, S.H. Chen, K.C. Chang, K.Y. Liu, A constitutive model of concrete confined by steel reinforcements and steel jackets, Can. J. Civ. Eng. 32 (1) (2005) 279–288.
[9] E. Choi, Y.S. Chung, J. Park, B.S. Cho, Behavior of reinforced concrete columns confined by new steel-jacketing method, ACI Struct. J. 107 (6) (2010) 654–662.
[10] E. Choi, Y.-S. Chung, K. Park, J.-S. Jeon, Effect of steel wrapping jackets on the bond strength of concrete and the lateral performance of circular RC columns, Eng. Struct. 48 (3) (2013) 43–54.
[11] U. Ersoy, T. Tankut, R. Suleiman, Behavior of jacketed columns, ACI Struct. J. 90 (3) (1993) 288–293.
[12] A.R. Takeuti, J.B. de Hanai, A. Mirmiran, Preloaded RC columns strengthened with high-strength concrete jacket under uniaxial compression, Mater. Struct. 41 (7) (2008) 1251–1262.
[13] K.G. Vandoros, S.E. Dritsos, Axial preloading effects when reinforced concrete columns are strengthened by concrete, Prog. Struct. Eng. Mater. 8 (3) (2006) 72–79.
[14] K.G. Vandoros, S.E. Dritsos, Concrete jacket construction detail effectiveness when strengthening RC columns, Constr. Build. Mater. 22 (3) (2008) 264–276.
[15] Vassilis K. Papanikolaou, Sotiria P. Stefanidou, Andreas J. Kappos, The effect of preloading on the strength of jacketed R/C columns, Constr. Build. Mater. 38 (1) (2013) 54–63.
[16] CEB-FIP MODEL CODE 2010 Volumn 1. Switzerland: International Federation for Structural Concrete (fib), March 2012.
[17] K. Sakino, H. Nakahara, Behavior of centrally loaded concrete-filled steel-tube short columns, J. Struct. Eng. 130 (2004) 180–188.
[18] J.B. Mander, M.J.N. Priestley, Theoretical stress-strain model for confined concrete, J. Struct. Eng. 114 (1988) 1807–1826.
[19] Z.H. Guo, C.Z. Wang, X.Q. Zhang, Investigation of strength and failure criterion ofconcrete under multi-axial stress, China Civ. Eng. J. 24 (3) (1991) 1–14 ([in Chinese]).
[20] F.E. Richart, A. Brandtzaeg, R.L. Brown, A study of the failure of concrete under combined compressive stresses. Bull. 185. Champaign (Ill): University of Illionis, Engineering Experimental Station, 1928.
[21] GB50010-2010, Code for Design of Concrete Structures, China Building Industry Press, Beijing, 2010 ([in Chinese]).
[22] H.T. Hu, C.S. Huang, M.H. Wu, Y.M. Wu, Nonlinear analysis of axially loaded concrete-filled tube columns with confinement effect, J. Struct. Eng. 129 (2003) 1322–1329.
[23] Y.Y. Lu, T.N. Gong, X.P. Zhang, J.F. Xue, Experimental research on behavior of circular RC column strengthened with self-compacting concrete filled circular steel jacket under axial loading, J. Build. Struct. 34 (6) (2013) 121–128 ([in Chinese]).
[24] CECS28:2012, Technical Specification for Concrete-filled Steel Tubular Structures, China Planning Press, Beijing, 2012 ([in Chinese]).
[25] ANSI/AISC 360-05, Specification for Structural Ssteel Buildings, American Institute of Steel Construction, Chicago, 2005.
[26] Eurocode 4 (EC4), Design of Steel and Concrete Structures. Part1 1: General Rules and Rules for Building, European Committee for Standardization, Brussels, 2004.
[27] Architectural Institute of Japan (AIJ), Recommendations for Design and Construction of Concrete Filled Steel Tubular Structures, Architectural Institute of Japan, Tokyo, 1997.